

Kerr-effect-based quantum logical gates in decoherence-free subspace

Fang-Fang Du*, Gang Fan, and Xue-Mei Ren

Science and Technology on Electronic Test and Measurement Laboratory, North University of China, Taiyuan 030051, China

The decoherence effect caused by the coupling between the system and the environment undoubtedly leads to the errors in efficient implementations of two (or three) qubit logical gates in quantum information processing. Fortunately, decoherence-free subspace (DFS) introduced can effectively decrease the influence of decoherence effect. In this paper, we propose some schemes for setting up a family of quantum control gates, including controlled-NOT (CNOT), Toffoli, and Fredkin gates for two or three logical qubits by means of cross-Kerr nonlinearities in DFS. These three logical gates require neither complicated quantum computational circuits nor auxiliary photons (or entangled states). The success probabilities of three logical gates are approximate 1 by performing the corresponding classical feed-forward operations based on the different measuring results of the X-homodyne detectors, and their fidelities are robust against the photon loss with the current technology. The proposed logical gates rely on only simple linear-optics elements, available single-qubit operations, and mature measurement methods, making our proposed gates be feasible and efficient in practical applications.

1 Introduction

Quantum computing, as a very sought-after technology, is used to tackle problems unsolvable by the best-of-breed classical computing [1, 2], which offers remarkable benefits, such as tremendous speedup [3], efficient searching for unordered

databases [4], large number factorization [5], and so on. Further, quantum computing is an imperative component of useful quantum information processing (QIP), making it ideal for adhibition in QIP [6–18]. The foundation of quantum computing is rest with quantum logical gates, which connect qubits and allow for applications of large-scale realization of quantum computation. The universal quantum gates [19], e.g., the two-qubit CNOT (controlled-NOT), three-qubit Toffoli (controlled-controlled-NOT), and Fredkin (controlled-swap) gates, can simplify complex quantum circuits to achieve the goals of QIP [20–22] with various quantum information platforms, such as linear optics [23–27], cross-Kerr nonlinearity [28–32], nitrogen-vacancy centers [33–35], quantum dots [36–38], waveguide systems [39–41], and neutral atoms [42, 43].

Nowadays, Google has alleged the quantum supremacy [44], unfortunately, the superconducting qubit processors are subjected to the loss of quantum coherence and the difficulty of scalability originated from expensive cryogenic apparatus strongly coupling to the realistic environment. That is, photon technologies have served relatively economical solutions, and photon-encoded qubits are also agreed with both low-decoherence applications and carriers to transmit the QIP. So far, some important progresses have been achieved in demonstrating the functionality of quantum logic gates for photon systems [23–26]. Additionally, the polarization degrees of freedom of photon system is easy to encode and manipulate with current optics techniques. However, the interference of environmental factors (i.e., atmospheric fluctuation, thermal and mechanical fluctuation, and birefringence in optical fibers) can lead to undesired interactions (harmful decoherence) in practical circumstances. These factors can cause errors in the transmission of polarized states of photons, making it necessary to

Fang-Fang Du*: dufangfang19871210@163.com

Gang Fan: fg18235091403@163.com

find useful ways to sidestep their impact on QIP. The decoherence-free subspace (DFS) approach has garnered significant attention to overcome the adverse effects of environmental noise factors on quantum information transmission, where DFS is a subspace of all quantum states in the unitary evolution of the quantum system. By utilizing two photons to encode a single logic qubit in DFS, i.e., $|\bar{0}\rangle = |H\rangle_1|V\rangle_2 = |HV\rangle$ and $|\bar{1}\rangle = |V\rangle_1|H\rangle_2 = |VH\rangle$ ($|H\rangle$ and $|V\rangle$ denote horizontally and vertically polarized states of photons, respectively) in Ref. [45]. After passing through a noisy channel, the state of the one photon is changed into $|H\rangle \xrightarrow{\text{transmission}} e^{i\gamma_1}|H\rangle$ and $|V\rangle \xrightarrow{\text{transmission}} e^{i\gamma_2}|V\rangle$. Then the evolution of the superposition state in the decoherence environment can be expressed as

$$\begin{aligned} & \alpha e^{i\gamma_1}|H\rangle + \beta e^{i\gamma_2}|V\rangle \\ &= e^{i\gamma_1}(\alpha|H\rangle + \beta e^{i(\gamma_2-\gamma_1)}|V\rangle) \\ &= \alpha|H\rangle + \beta e^{i\gamma}|V\rangle, \end{aligned} \quad (1)$$

where $\gamma = \gamma_2 - \gamma_1$. Afterward, the evolution of the state in DFS can be illustrated as

$$\begin{aligned} \alpha|\bar{0}\rangle + \beta|\bar{1}\rangle &= \alpha|H\rangle_1|V\rangle_2 + \beta|V\rangle_1|H\rangle_2 \\ &\rightarrow \alpha|H\rangle_1 e^{i\gamma}|V\rangle_2 + \beta e^{i\gamma}|V\rangle_1|H\rangle_2 \\ &= e^{i\gamma}(\alpha|H\rangle_1|V\rangle_2 + \beta|V\rangle_1|H\rangle_2) \\ &= \alpha|\bar{0}\rangle + \beta|\bar{1}\rangle. \end{aligned} \quad (2)$$

Obviously, it is noted that DFS can effectively avoid the influence of collective dephasing noise. Therefore, quantum states encoded on the DFS are robust against certain types of noise and decoherence processes. This resilience makes DFS to have applications in various areas of QIP, including the construction of the quantum network [46], the valid preparation and the conversion of the quantum states [47–51], and quantum teleportation [52, 53], quantum computation [54–56], and quantum sensing [57, 58]. They offer a promising avenue for mitigating the effects of decoherence and improving the reliability of quantum technologies.

In this paper, in view of the cross-Kerr nonlinearity, we present some schemes for setting up a family of quantum control gates, including CNOT, Toffoli, and Fredkin gates in DFS for polarization-encoded logical qubits of photon systems, which has the advantages over low-decoherence character, flexible single-qubit ma-

nipulation, and ultra-fast transmission. The employment of two key tools, i.e., a SWAP gate (abbreviated as S) and a path coupler, are innovated for implementing three logical gates. The former with the success probability of 1 relies on only simple linear-optics elements, which swaps not only the polarized states of two photons but also two paths of a single photon. The latter with the probability near close to 1 is utilized to combine two paths of a photon to the one by available single-qubit operations and mature measurement methods, which halves the number of the paths of the photon and greatly simplifies the quantum circuit. Therefore, these three logical gates require neither complicated quantum computational circuits nor auxiliary photons (or entangled states). The success probabilities of three logical gates are approximate 1 by performing the corresponding classical feed-forward operations based on the different measuring results of the X-homodyne detectors, and their fidelities are robust against the photon loss with the current technology.

2 SWAP gate and path coupler

Nowadays, to break up the limitation on the success probabilities less than 1 of the quantum gates with linear optics [23–26], the cross-Kerr nonlinearity [28–31, 59] has provided a potential solution for improving the success probability of the quantum gate, as it has the potential available to an evolution of the combined system composed of n photons and a coherent state but without destroying the involved photon. Let us assume that $|n\rangle_i$ represents a state of n photons (signal), and the probe beam is in a coherent state $|\alpha\rangle_P$. After passing through the interaction U_K of cross-Kerr nonlinearity, the conditional phase shift between a signal system and probe beam as follows:

$$U_K|n\rangle_i|\alpha\rangle_P = e^{-i\frac{t}{\hbar}\hat{H}}|n\rangle_1|\alpha\rangle_P = |n\rangle_1|\alpha e^{in\theta}\rangle, \quad (3)$$

where $\hat{H} = \hbar\chi N_1 N_2$ is the interaction Hamiltonian of cross-Kerr nonlinearity. The Kerr effect varies with different media and χ represents the strength of nonlinearity. N_1 and N_2 are photon number operators of signal and probe modes, respectively. $\theta = \chi t$ is the phase shift and t is the interaction time in Kerr medium. $|n\rangle$ is the n -photon state, and $|\alpha\rangle = e^{-|\alpha|^2/2} \sum_{n=0}^{\infty} [\alpha^n / \sqrt{n!}] |n\rangle$

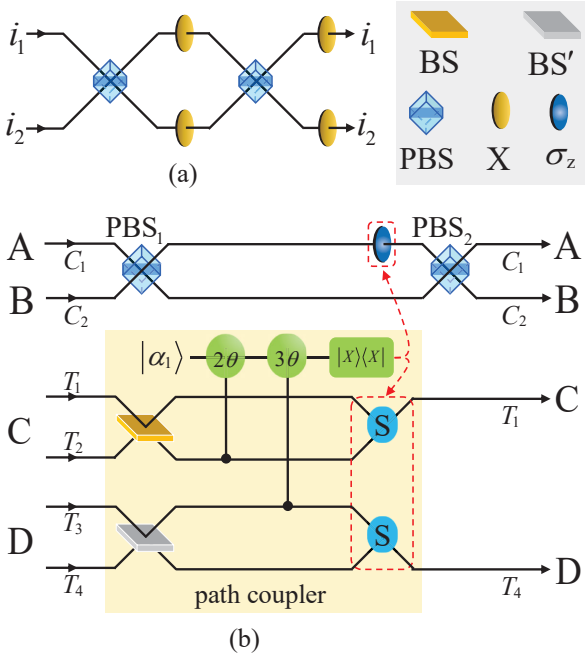


Figure 1: (a) Schematic diagram of a SWAP gate (abbreviated as S) swapping the polarized states of two photons and two paths of a single photon as well. (b) Schematic diagram of a path coupler to combine two paths into one without destroying the polarization information. BS represents a 50 : 50 beam splitter, which completes the paths transformation between up and down paths (i_{up}, i_{down}), $i_{up} \rightarrow (i_{up} + i_{down})/\sqrt{2}$, $i_{down} \rightarrow (i_{up} - i_{down})/\sqrt{2}$, while the other BS' completes the transformation $i_{up} \rightarrow (i_{down} - i_{up})/\sqrt{2}$, $i_{down} \rightarrow (i_{up} + i_{down})/\sqrt{2}$. Polarization beam splitters (PBSs) transmit the $|H\rangle$ -polarized component and reflect the $|V\rangle$ -polarized one of the photon. The X fulfills the bit-flip operation $|H\rangle \leftrightarrow |V\rangle$ and the σ_z fulfills the phase-flip operation $\sigma_z = |H\rangle\langle H| - |V\rangle\langle V|$.

is the coherent state of probe field.

2.1 SWAP gate

The SWAP gate (abbreviated as S), depicted in Figure 1a, serves two functions. The one is to exchange two paths of a single photon and the other one is to swap the polarized states of two photons. In detail, suppose that the input photon 1 and photon 2 are initially in the following state

$$|S\rangle_0 = (\xi_1|H\rangle + \xi_2|V\rangle)_1|i_1\rangle \otimes (\epsilon_1|H\rangle + \epsilon_2|V\rangle)_2|i_2\rangle, \quad (4)$$

where i_1 and i_2 represent the paths of input photon 1 and photon 2, respectively. The complex coefficients conform to the normalization principle, i.e., $|\xi_1|^2 + |\xi_2|^2 = 1$ and $|\epsilon_1|^2 + |\epsilon_2|^2 = 1$. After

the input photon 1 and photon 2 pass through the optical elements polarization beam splitters (PBSs), which transmit the $|H\rangle$ -polarized component and reflect the $|V\rangle$ -polarized one of the photon, and Xs, where half wave plates oriented at 45° can fulfill the bit-flip operation $|H\rangle \leftrightarrow |V\rangle$, the parallel transformation can be obtained

$$|S\rangle_1 = (\epsilon_1|H\rangle + \epsilon_2|V\rangle)_2|i_1\rangle \otimes (\xi_1|H\rangle + \xi_2|V\rangle)_1|i_2\rangle. \quad (5)$$

Based on Eq. (5), the quantum circuit unequivocally swaps the polarized states of two photons 12 only with simple linear-optics elements. Additionally, the S has another function, which can swap two paths of a single photon, as the single photon enters from the up (down) path $|i_1\rangle$ ($|i_2\rangle$) and then exits from the down (up) one $|i_2\rangle$ ($|i_1\rangle$).

2.2 Path coupler

A path coupler shown in Figure 1b, called a quantum eraser, combines two paths into one, making halve the number of the paths without destroying the polarization information of the photon. Suppose that the state of two photons AB to encode a logic qubit and the state of two photons CD to encode another logic qubit in DFS are

$$\begin{aligned} |\phi\rangle_{AB} &= \beta_1|\bar{0}\rangle + \beta_2|\bar{1}\rangle, \\ |\phi\rangle_{CD} &= \delta_1|\bar{0}\rangle + \delta_2|\bar{1}\rangle, \end{aligned} \quad (6)$$

where the complex coefficients conforms to the normalization principle, i.e., $|j_1|^2 + |j_2|^2 = 1$, ($j = \beta, \delta$). Four photons ABCD are initially prepared in the arbitrary state

$$|\Gamma\rangle_0 = \beta_1|\bar{0}\rangle_{AB}|\phi\rangle_{CD}|C_1C_2\rangle|T_1T_4\rangle + \beta_2|\bar{1}\rangle_{AB}|\phi\rangle_{CD}|C_1C_2\rangle|T_2T_3\rangle. \quad (7)$$

Here, (C_1, C_2) represent the paths of photon AB. (T_1, T_2) and (T_3, T_4) represent the paths of photon C and photon D, respectively.

Firstly, photons AB pass through PBS₁, meanwhile photons CD pass through 50 : 50 beam splitters, i.e., BS and BS', where BS completes the paths transformation between up path i_{up} and down path i_{down} : $i_{up} \rightarrow (i_{up} + i_{down})/\sqrt{2}$, $i_{down} \rightarrow (i_{up} - i_{down})/\sqrt{2}$, while BS' completes the transformation: $i_{up} \rightarrow (i_{down} - i_{up})/\sqrt{2}$, $i_{down} \rightarrow (i_{up} + i_{down})/\sqrt{2}$, respectively.

The system state is changed into

$$\begin{aligned}
|\Gamma\rangle'_0 &= \beta_1|\bar{0}\rangle_{AB}|\phi\rangle_{CD}|C_1C_2\rangle \\
&\otimes(|T_1T_3\rangle + |T_1T_4\rangle + |T_2T_3\rangle + |T_2T_4\rangle) \\
&+ \beta_2|\bar{1}\rangle_{AB}|\phi\rangle_{CD}|C_1C_2\rangle \\
&\otimes(|T_1T_4\rangle - |T_1T_3\rangle - |T_2T_4\rangle + |T_2T_3\rangle).
\end{aligned} \tag{8}$$

Then the photons CD interact with the coherent state $|\alpha\rangle_1$ via Kerr media, based on Eq. (3), the process can be expressed as

$$\begin{aligned}
|\Gamma\rangle_1 &= \frac{1}{2}(\beta_1|\bar{0}\rangle_{AB}|\phi\rangle_{CD}|C_2\rangle|T_1T_4\rangle \\
&+ \beta_2|\bar{1}\rangle_{AB}|\phi\rangle_{CD}|C_1\rangle|T_1T_4\rangle)|\alpha_1\rangle \\
&+ (\beta_1|\bar{0}\rangle_{AB}|\phi\rangle_{CD}|C_2\rangle|T_2T_4\rangle \\
&- \beta_2|\bar{1}\rangle_{AB}|\phi\rangle_{CD}|C_1\rangle|T_2T_4\rangle)|\alpha_1e^{2i\theta}\rangle \\
&+ (\beta_1|\bar{0}\rangle_{AB}|\phi\rangle_{CD}|C_2\rangle|T_1T_3\rangle \\
&- \beta_2|\bar{1}\rangle_{AB}|\phi\rangle_{CD}|C_1\rangle|T_1T_3\rangle)|\alpha_1e^{3i\theta}\rangle \\
&+ (\beta_1|\bar{0}\rangle_{AB}|\phi\rangle_{CD}|C_2\rangle|T_2T_3\rangle \\
&+ \beta_2|\bar{1}\rangle_{AB}|\phi\rangle_{CD}|C_1\rangle|T_2T_3\rangle)|\alpha_1e^{5i\theta}\rangle.
\end{aligned} \tag{9}$$

After following the X-homodyne measurement, the interaction of the cross-Kerr nonlinearity can induce four measurement outcomes, i.e., phase shifts 0 , 2θ , 3θ and 5θ . If the outcome is zero phase shift, the state of the whole system becomes into

$$\begin{aligned}
|\Gamma\rangle_2 &= (\beta_1|\bar{0}\rangle_{AB}|C_2\rangle + \beta_2|\bar{1}\rangle_{AB}|C_1\rangle) \\
&\otimes|\phi\rangle_{CD}|T_1T_4\rangle.
\end{aligned} \tag{10}$$

If the outcome is another case, corresponding feed-forward operations shown in Table 1 must be performed based on the measurement outcomes to get the desirous state in Eq. (10). In Table 1, I_{T_1,T_2} (I_{T_3,T_4}) represents the paths T_1, T_2 (T_3, T_4) of photons C (or D) to remain unchanged, S_{T_1,T_2} (S_{T_3,T_4}) mean to swap two paths of the photon C (or D) with the S in Figure 1a, and σ_z performs the phase-flip operation $\sigma_z = |H\rangle\langle H| - |V\rangle\langle V|$ from the path C_1 .

Finally, photons AB pass through the PBS_2 , resulting in the final state

$$|\Gamma\rangle_3 = (\beta_1|\bar{0}\rangle + \beta_2|\bar{1}\rangle)_{AB}|\phi\rangle_{CD}|C_1C_2\rangle|T_1T_4\rangle. \tag{11}$$

That is, the path coupler merges two paths T_1 and T_2 (T_3 and T_4) into the one T_1 (T_4) with the above device, and likewise, as the quantum circuit in Figure 1a is universal and flexible, the

Table 1: The measurement results of the coherent state $|\alpha\rangle_1$, and the corresponding single-qubit feed-forward operations.

Measurement results	Single-qubit operations
0	$I_{T_1,T_2} \otimes I_{T_3,T_4}$
2θ	$(\sigma_z)_{C_1} \otimes I_{T_1,T_2} \otimes S_{T_3,T_4}$
3θ	$(\sigma_z)_{C_1} \otimes S_{T_1,T_2} \otimes I_{T_3,T_4}$
5θ	$S_{T_1,T_2} \otimes S_{T_3,T_4}$

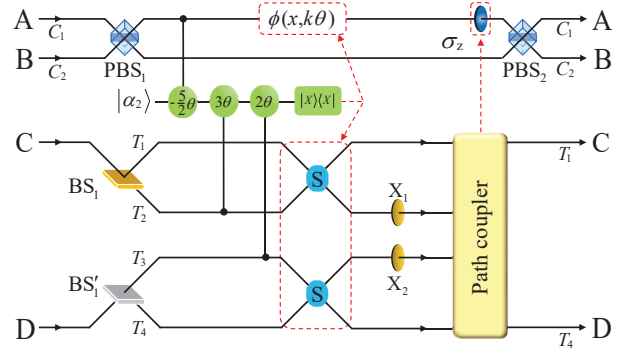


Figure 2: Schematic diagram of the CNOT gate based on cross-Kerr nonlinearities in DFS. $\phi(x, k\theta)$ ($k = 2, 3, 5$) represents the phase modulation.

merging of other paths we desired can be obtained by suitable feed-forward operations, such as T_1 and T_2 (T_3 and T_4) are merged into the path T_2 (T_3). Similarly, when the initial state of two photons CD to encode logic qubit in DFS is $|\bar{\phi}\rangle_{CD} = \delta_1|\bar{1}\rangle + \delta_2|\bar{0}\rangle$, by replacing $|\phi\rangle_{CD}$ with $|\bar{\phi}\rangle_{CD}$ in Eq. (7), we also obtain the same appearance. That is, whether the initial state is $|\phi\rangle_{CD}$ or $|\bar{\phi}\rangle_{CD}$, the path coupler can merges two paths into one.

3 Quantum logical gate

3.1 CNOT gate

Suppose that the initial state of two logical qubits in DFS is $|\Omega\rangle_0 = |\phi\rangle_{AB} \otimes |\phi\rangle_{CD}$, where the quantum state $|\phi\rangle_{AB}$ of control logical qubit AB and that $|\phi\rangle_{CD}$ of target logical qubit CD are the same as those in Eq. (6). The quantum circuit for implementing the CNOT gate is shown in Figure 2. Firstly, the control photons AB pass through PBS_1 , meanwhile the target photons CD pass through BS_1 and BS'_1 , respectively. Then, four photons combine with the coherent state $|\alpha\rangle_2$ with the help of the cross-Kerr non-

linearity, resulting in the quantum state $|\Omega\rangle_0 = |\phi\rangle_{AB} \otimes |\phi\rangle_{CD} \otimes |\alpha_2\rangle$ changed into the state

$$\begin{aligned}
|\Omega\rangle_1 = & \frac{1}{2} [(\beta_1|HV\rangle_{AB}|\phi\rangle_{CD}|C_2\rangle|T_1T_4\rangle \\
& + \beta_2|VH\rangle_{AB}|\phi\rangle_{CD}|C_1\rangle|T_2T_3\rangle)|\alpha_2\rangle \\
& + (\beta_1|HV\rangle_{AB}|\phi\rangle_{CD}|C_2\rangle|T_1T_3\rangle|\alpha_2e^{2i\theta}\rangle \\
& + \beta_2|VH\rangle_{AB}|\phi\rangle_{CD}|C_1\rangle|T_2T_4\rangle|\alpha_2e^{-2i\theta}\rangle) \\
& + (\beta_1|HV\rangle_{AB}|\phi\rangle_{CD}|C_2\rangle|T_2T_4\rangle|\alpha_2e^{3i\theta}\rangle \\
& + \beta_2|VH\rangle_{AB}|\phi\rangle_{CD}|C_1\rangle|T_1T_3\rangle|\alpha_2e^{-3i\theta}\rangle) \\
& + (\beta_1|HV\rangle_{AB}|\phi\rangle_{CD}|C_2\rangle|T_2T_3\rangle|\alpha_2e^{5i\theta}\rangle \\
& + \beta_2|VH\rangle_{AB}|\phi\rangle_{CD}|C_1\rangle|T_1T_4\rangle|\alpha_2e^{-5i\theta}\rangle)]. \quad (12)
\end{aligned}$$

As the X-homodyne measurement cannot distinguish between phase shift $k\theta$ and phase shift $-k\theta$ ($k = 2, 3, 5$), we obtain four different scenarios of phase shifts ($0, \pm 2\theta, \pm 3\theta, \pm 5\theta$). A phase modulation $\phi(x, k\theta) = \alpha \sin k\theta(x - 2\alpha \cos k\theta) \bmod 2\pi$ ($k = 2, 3, 5$), a function of the phase shift and the eigenvalue x of the X-homodyne operator, is performed to erase the phase difference between the two superposition terms in the scenarios of three different nonzero phase shifts. If the outcome is zero phase shift, the state of the whole system becomes into

$$\begin{aligned}
|\Omega\rangle'_1 = & \beta_1|HV\rangle_{AB}|\phi\rangle_{CD}|C_2\rangle|T_1T_4\rangle \\
& + \beta_2|VH\rangle_{AB}|\phi\rangle_{CD}|C_1\rangle|T_2T_3\rangle. \quad (13)
\end{aligned}$$

By performing corresponding feed-forward operations for the other measurement outcomes, as shown in Table 2, we can get the state $|\Omega\rangle_1$ with the success probability close to 1.

Next, the target photons CD pass through X_1 and X_2 on paths T_2 and T_3 , respectively, and the evolution of the system can be illustrated as follows

$$\begin{aligned}
|\Omega\rangle_2 = & \beta_1|\bar{0}\rangle_{AB}|\phi\rangle_{CD}|C_2\rangle|T_1T_4\rangle \\
& + \beta_2|\bar{1}\rangle_{AB}|\bar{\phi}\rangle_{CD}|C_1\rangle|T_2T_3\rangle. \quad (14)
\end{aligned}$$

Finally, the control photons AB pass through PBS_2 and the target photons CD pass through

the path coupler in Figure 1b, merging two paths T_1 and T_2 (T_3 and T_4) into one path T_1 (T_4) of the target photon C (D), the quantum state $|\Omega\rangle_2$ is evolved as

$$\begin{aligned}
|\Omega\rangle_3 = & (\beta_1|\bar{0}\rangle_{AB}|\phi\rangle_{CD} + \beta_2|\bar{1}\rangle_{AB}|\bar{\phi}\rangle_{CD}) \\
& \otimes |C_1C_2\rangle|T_1T_4\rangle. \quad (15)
\end{aligned}$$

Table 2: The measurement results of the coherent state $|\alpha_2\rangle$, and the corresponding single-qubit feed-forward operations.

Measurement results	Phase modulation	Single-qubit operations
0	0	$I_{T_1, T_2} \otimes I_{T_3, T_4}$
$\pm 2\theta$	$\phi(x, 2\theta)_{C_1}$	$I_{T_1, T_2} \otimes S_{T_3, T_4}$
$\pm 3\theta$	$\phi(x, 3\theta)_{C_1}$	$S_{T_1, T_2} \otimes I_{T_3, T_4}$
$\pm 5\theta$	$\phi(x, 5\theta)_{C_1}$	$S_{T_1, T_2} \otimes S_{T_3, T_4}$

It is obvious that the result of the CNOT gate flips the state of the target photons CD if and only if the control photons AB is in the state $|\bar{1}\rangle_{AB}$, and has no change otherwise.

3.2 Toffoli gate

The quantum circuit of the three-logic-qubit Toffoli gate composed of six photons in Figure 3, where the initial state of the second control qubit encoded by two photons EF in DFS is $|\phi\rangle_{EF} = \gamma_1|\bar{0}\rangle + \gamma_2|\bar{1}\rangle$ ($|\gamma_1|^2 + |\gamma_2|^2 = 1$). Firstly, the control photons AB and the target ones CD perform the same operations as the first step of two-logic-qubit CNOT gate in Figure 2. By performing corresponding feed-forward operations as shown in Table 2, we can get quantum state $|\Phi\rangle_1$ with the same form in Eq. (13) with the success probability close to 1. Now, the system state can be expressed as $|\Phi\rangle_1 = \beta_1|HV\rangle_{AB}|\phi\rangle_{EF}|\phi\rangle_{CD}|C_2\rangle|C_3C_4\rangle|T_1T_4\rangle + \beta_2|VH\rangle_{AB}|\phi\rangle_{EF}|\phi\rangle_{CD}|C_1\rangle|C_3C_4\rangle|T_2T_3\rangle$.

Secondly, the second control photons EF enter into PBS_2 , meanwhile the target photons CD enter into (BS_2, BS'_2) and BS_3 and BS'_3 , and their evolution interacting with the coherent state α_4 via Kerr media can be expressed as

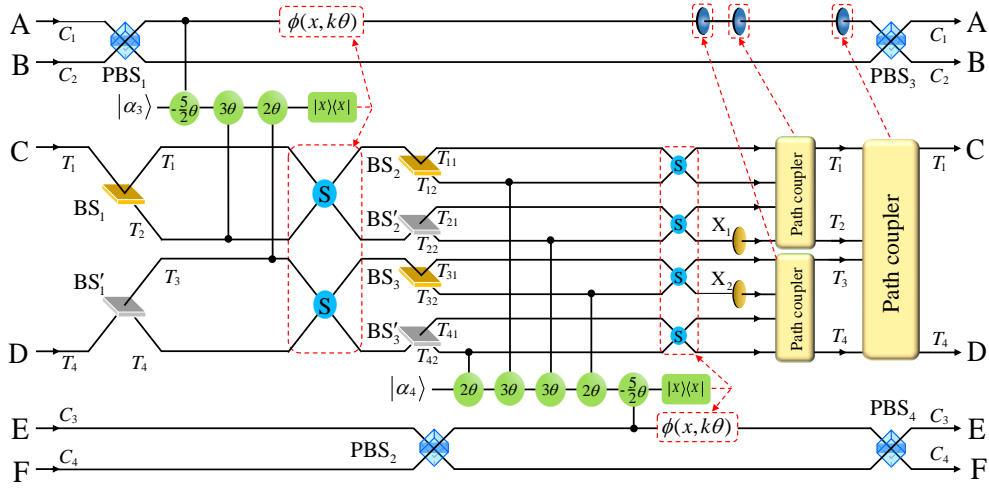


Figure 3: Schematic diagram of the Toffoli gate in DFS based on cross-Kerr nonlinearities.

$$\begin{aligned}
|\Phi\rangle_2 = & (\beta_1\gamma_1|HV\rangle_{AB}|HV\rangle_{EF}|\phi\rangle_{CD}|C_2\rangle|C_4\rangle|T_{11}T_{41}\rangle \\
& +\beta_2\gamma_1|VH\rangle_{AB}|HV\rangle_{EF}|\phi\rangle_{CD}|C_1\rangle|C_4\rangle|T_{21}T_{31}\rangle \\
& +\beta_1\gamma_2|HV\rangle_{AB}|VH\rangle_{EF}|\phi\rangle_{CD}|C_2\rangle|C_3\rangle|T_{12}T_{42}\rangle \\
& +\beta_2\gamma_2|VH\rangle_{AB}|VH\rangle_{EF}|\phi\rangle_{CD}|C_1\rangle|C_3\rangle|T_{22}T_{32}\rangle)|\alpha_4\rangle \\
& +[(\beta_1\gamma_1|HV\rangle_{AB}|HV\rangle_{EF}|\phi\rangle_{CD}|C_2\rangle|C_4\rangle|T_{11}T_{42}\rangle \\
& +\beta_2\gamma_1|VH\rangle_{AB}|HV\rangle_{EF}|\phi\rangle_{CD}|C_1\rangle|C_4\rangle|T_{21}T_{32}\rangle)|\alpha_4e^{2i\theta}\rangle \\
& +(\beta_1\gamma_2|HV\rangle_{AB}|VH\rangle_{EF}|\phi\rangle_{CD}|C_2\rangle|C_3\rangle|T_{12}T_{41}\rangle \\
& +\beta_2\gamma_2|VH\rangle_{AB}|VH\rangle_{EF}|\phi\rangle_{CD}|C_1\rangle|C_3\rangle|T_{22}T_{31}\rangle)]|\alpha_4e^{-2i\theta}\rangle \\
& +[(\beta_1\gamma_1|HV\rangle_{AB}|HV\rangle_{EF}|\phi\rangle_{CD}|C_2\rangle|C_4\rangle|T_{12}T_{41}\rangle \\
& +\beta_2\gamma_1|VH\rangle_{AB}|HV\rangle_{EF}|\phi\rangle_{CD}|C_1\rangle|C_4\rangle|T_{22}T_{31}\rangle)|\alpha_4e^{3i\theta}\rangle \\
& +(\beta_1\gamma_2|HV\rangle_{AB}|VH\rangle_{EF}|\phi\rangle_{CD}|C_2\rangle|C_3\rangle|T_{11}T_{42}\rangle \\
& +\beta_2\gamma_2|VH\rangle_{AB}|VH\rangle_{EF}|\phi\rangle_{CD}|C_1\rangle|C_3\rangle|T_{21}T_{32}\rangle)]|\alpha_4e^{-3i\theta}\rangle \\
& +[(\beta_1\gamma_1|HV\rangle_{AB}|HV\rangle_{EF}|\phi\rangle_{CD}|C_2\rangle|C_4\rangle|T_{12}T_{42}\rangle \\
& +\beta_2\gamma_1|VH\rangle_{AB}|HV\rangle_{EF}|\phi\rangle_{CD}|C_1\rangle|C_4\rangle|T_{22}T_{32}\rangle)|\alpha_4e^{5i\theta}\rangle \\
& +(\beta_1\gamma_2|HV\rangle_{AB}|VH\rangle_{EF}|\phi\rangle_{CD}|C_2\rangle|C_3\rangle|T_{11}T_{41}\rangle \\
& +\beta_2\gamma_2|VH\rangle_{AB}|VH\rangle_{EF}|\phi\rangle_{CD}|C_1\rangle|C_3\rangle|T_{21}T_{31}\rangle)]|\alpha_4e^{-5i\theta}\rangle.
\end{aligned} \tag{16}$$

After performing the X-homodyne measurement on the coherent state α_4 , we once again obtain four sets of measurement outcomes, and corresponding feed-forward operations shown in Table 3 are executed based on the measurement outcomes, resulting in the quantum state $|\Phi\rangle_2$ collapses into

$$\begin{aligned}
|\Phi\rangle'_2 = & \beta_1\gamma_1|HV\rangle_{AB}|HV\rangle_{EF}|\phi\rangle_{CD}|C_2\rangle|C_4\rangle|T_{11}T_{41}\rangle \\
& +\beta_2\gamma_1|VH\rangle_{AB}|HV\rangle_{EF}|\phi\rangle_{CD}|C_1\rangle|C_4\rangle|T_{21}T_{31}\rangle \\
& +\beta_1\gamma_2|HV\rangle_{AB}|VH\rangle_{EF}|\phi\rangle_{CD}|C_2\rangle|C_3\rangle|T_{12}T_{42}\rangle \\
& +\beta_2\gamma_2|VH\rangle_{AB}|VH\rangle_{EF}|\phi\rangle_{CD}|C_1\rangle|C_3\rangle|T_{22}T_{32}\rangle.
\end{aligned}$$

Thirdly, the target photons CD pass through X_1 and X_2 , respectively. The evolution of the system can be illustrated as follows

$$\begin{aligned}
|\Phi\rangle_3 = & \beta_1\gamma_1|HV\rangle_{AB}|HV\rangle_{EF}|\phi\rangle_{CD}|C_2\rangle|C_4\rangle|T_{11}T_{41}\rangle \\
& +\beta_2\gamma_1|VH\rangle_{AB}|HV\rangle_{EF}|\phi\rangle_{CD}|C_1\rangle|C_4\rangle|T_{21}T_{31}\rangle \\
& +\beta_1\gamma_2|HV\rangle_{AB}|VH\rangle_{EF}|\phi\rangle_{CD}|C_2\rangle|C_3\rangle|T_{12}T_{42}\rangle \\
& +\beta_2\gamma_2|VH\rangle_{AB}|VH\rangle_{EF}|\phi\rangle_{CD}|C_1\rangle|C_3\rangle|T_{22}T_{32}\rangle.
\end{aligned} \tag{18}$$

Fourthly, the target photons CD pass through the two path couplers in Figure 1b, merging the (17)paths (T_{11}, T_{12}) , (T_{21}, T_{22}) , (T_{31}, T_{32}) and $(T_{41},$

Table 3: The measurement results of the coherent state $|\alpha_4\rangle$, and the corresponding single-qubit feed-forward operations.

Measurement results	Phase modulation	Single-qubit operations
0	0	$I_{T_{11},T_{12}} \otimes I_{T_{21},T_{22}} \otimes I_{T_{31},T_{32}} \otimes I_{T_{41},T_{42}}$
$\pm 2\theta$	$\phi(x, 2\theta)_{C_3}$	$I_{T_{11},T_{12}} \otimes I_{T_{21},T_{22}} \otimes S_{T_{31},T_{32}} \otimes S_{T_{41},T_{42}}$
$\pm 3\theta$	$\phi(x, 3\theta)_{C_3}$	$S_{T_{11},T_{12}} \otimes S_{T_{21},T_{22}} \otimes I_{T_{31},T_{32}} \otimes I_{T_{41},T_{42}}$
$\pm 5\theta$	$\phi(x, 5\theta)_{C_3}$	$S_{T_{11},T_{12}} \otimes S_{T_{21},T_{22}} \otimes S_{T_{31},T_{32}} \otimes S_{T_{41},T_{42}}$

T_{42}) into the paths T_1, T_2, T_3 and T_4 , respectively. Then, the quantum state becomes into

$$\begin{aligned}
|\Phi\rangle_4 = & \beta_1\gamma_1|HV\rangle_{AB}|HV\rangle_{EF}|\phi\rangle_{CD}|C_2\rangle|C_4\rangle|T_1T_4\rangle \\
& + \beta_2\gamma_1|VH\rangle_{AB}|HV\rangle_{EF}|\phi\rangle_{CD}|C_1\rangle|C_4\rangle|T_2T_3\rangle \\
& + \beta_1\gamma_2|HV\rangle_{AB}|VH\rangle_{EF}|\phi\rangle_{CD}|C_2\rangle|C_3\rangle|T_1T_4\rangle \\
& + \beta_2\gamma_2|VH\rangle_{AB}|VH\rangle_{EF}|\phi\rangle_{CD}|C_1\rangle|C_3\rangle|T_2T_3\rangle.
\end{aligned} \tag{19}$$

Finally, the target photons qubits CD pass through the third path coupler again, merging paths T_1 and T_2 (T_3 and T_4) into paths T_1 (T_4), and meanwhile the control photons AB and EF pass through PBS₃ and PBS₄, respectively, resulting into

$$\begin{aligned}
|\Phi\rangle_5 = & (\beta_1\gamma_1|HV\rangle_{AB}|HV\rangle_{EF}|\phi\rangle_{CD} \\
& + \beta_2\gamma_1|VH\rangle_{AB}|HV\rangle_{EF}|\phi\rangle_{CD} \\
& + \beta_1\gamma_2|HV\rangle_{AB}|VH\rangle_{EF}|\phi\rangle_{CD} \\
& + \beta_2\gamma_2|VH\rangle_{AB}|VH\rangle_{EF}|\phi\rangle_{CD}) \\
& \otimes |C_1C_2\rangle|C_3C_4\rangle|T_1T_4\rangle \\
= & (\beta_1\gamma_1|\bar{0}\rangle_{AB}|\bar{0}\rangle_{EF}|\phi\rangle_{CD} \\
& + \beta_1\gamma_2|\bar{0}\rangle_{AB}|\bar{1}\rangle_{EF}|\phi\rangle_{CD} \\
& + \beta_2\gamma_1|\bar{1}\rangle_{AB}|\bar{0}\rangle_{EF}|\phi\rangle_{CD} \\
& + \beta_2\gamma_2|\bar{1}\rangle_{AB}|\bar{1}\rangle_{EF}|\phi\rangle_{CD}) \\
& \otimes |C_1C_2\rangle|C_3C_4\rangle|T_1T_4\rangle.
\end{aligned} \tag{20}$$

Apparently, based on Eq. (20) the three-logic-qubit Toffoli gate encoding with six photons ABCDEF in DFS is fulfilled perfectly with the success probability close to 1, by performing appropriate feed-forward operations in Tables 1-3, where the Toffoli gate flips the states of the target photons CD if and only if the control photons

AB and EF are both in the state $|\bar{1}\rangle_{AB}|\bar{1}\rangle_{EF}$, and has no change otherwise.

3.3 Fredkin gate

The quantum circuit of the three-logic-qubit Fredkin gate is depicted in Figure 4, where the initial states of three logical qubits are the same as the one of the Toffoli gate, with four photons CD and EF serving as two target logical qubits and photons AB as a unique control logical qubit. Firstly, four target photons CDEF traverse BS₁, BS'₁, BS₂, and BS'₂, respectively, and then undergo the cross-Kerr nonlinearity. The evolution of system is illustrated by

$$\begin{aligned}
|\Psi\rangle_1 = & |\phi\rangle_{AB}|\phi\rangle_{CD}|\phi\rangle_{EF}|C_1C_2\rangle|T_1T_4\rangle|T_5T_8\rangle \\
\stackrel{kerr}{\rightarrow} & |\phi\rangle_{AB} \otimes |\phi\rangle_{CD} \otimes |\phi\rangle_{EF} \\
& \otimes (|C_1C_2\rangle|T_1T_4\rangle|T_5T_8\rangle|\alpha_5\rangle \\
& + |C_1C_2\rangle|T_2T_3\rangle|T_6T_7\rangle|\alpha_5\rangle \\
& + |C_1C_2\rangle|T_2T_4\rangle|T_5T_8\rangle|\alpha_5e^{i\theta}\rangle \\
& + |C_1C_2\rangle|T_1T_3\rangle|T_6T_7\rangle|\alpha_5e^{-i\theta}\rangle \\
& + |C_1C_2\rangle|T_1T_3\rangle|T_5T_8\rangle|\alpha_5e^{2i\theta}\rangle \\
& + |C_1C_2\rangle|T_2T_4\rangle|T_6T_7\rangle|\alpha_5e^{-2i\theta}\rangle \\
& + |C_1C_2\rangle|T_2T_3\rangle|T_5T_8\rangle|\alpha_5e^{3i\theta}\rangle \\
& + |C_1C_2\rangle|T_1T_4\rangle|T_6T_7\rangle|\alpha_5e^{-3i\theta}\rangle \\
& + |C_1C_2\rangle|T_1T_4\rangle|T_6T_8\rangle|\alpha_5e^{4i\theta}\rangle \\
& + |C_1C_2\rangle|T_2T_3\rangle|T_5T_7\rangle|\alpha_5e^{-4i\theta}\rangle \\
& + |C_1C_2\rangle|T_2T_4\rangle|T_6T_8\rangle|\alpha_5e^{5i\theta}\rangle \\
& + |C_1C_2\rangle|T_1T_3\rangle|T_5T_7\rangle|\alpha_5e^{-5i\theta}\rangle \\
& + |C_1C_2\rangle|T_1T_3\rangle|T_6T_8\rangle|\alpha_5e^{6i\theta}\rangle \\
& + |C_1C_2\rangle|T_2T_4\rangle|T_5T_7\rangle|\alpha_5e^{-6i\theta}\rangle \\
& + |C_1C_2\rangle|T_2T_3\rangle|T_6T_8\rangle|\alpha_5e^{7i\theta}\rangle \\
& + |C_1C_2\rangle|T_1T_4\rangle|T_5T_7\rangle|\alpha_5e^{-7i\theta}\rangle).
\end{aligned} \tag{21}$$

If the outcome is zero phase shift, the state of the composite system can be denoted as

$$\begin{aligned}
|\Psi\rangle'_1 = & |\phi\rangle_{AB}|\phi\rangle_{CD}|\phi\rangle_{EF}(|C_1C_2\rangle|T_1T_4\rangle|T_5T_8\rangle \\
& + |C_1C_2\rangle|T_2T_3\rangle|T_6T_7\rangle).
\end{aligned} \tag{22}$$

Otherwise, nonzero phase shifts ($\pm\theta, \pm 2\theta, \dots, \pm 7\theta$) are obtained. The phase shift $2\phi(x, q\theta)$ ($q = 1, \dots, 7$) operation should be performed, along with the corresponding feed-forward single-qubit operations as shown in Table 4 to achieve the desired state in Eq. (22).

Secondly, the control photons AB traverse PBS₁, and the evolution process of they interacting with the coherent state $|\alpha_6\rangle$ is expressed

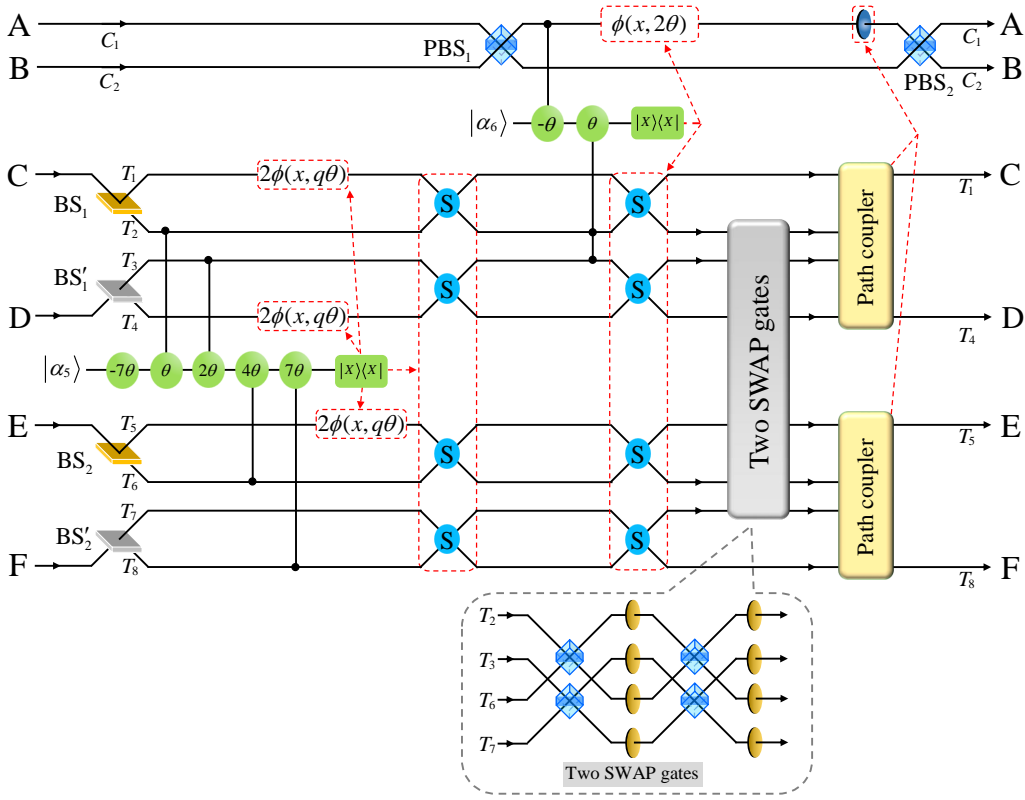


Figure 4: Schematic diagram of the Fredkin gate in DFS based on cross-Kerr nonlinearities. $2\phi(x, q\theta)$ ($q = 1, 2, \dots, 7$) represents the phase modulation.

Table 4: The measurement results of the coherent state $|\alpha_5\rangle$, and the corresponding single-qubit feed-forward operations.

Measurement results	Phase modulation	Single-qubit operations
0	0	I_{T_1, T_2} $\otimes I_{T_3, T_4} \otimes I_{T_5, T_6}$
$\pm\theta$	$2\phi(x, \theta)_{T_1}$	S_{T_1, T_2} $\otimes I_{T_3, T_4} \otimes I_{T_5, T_6}$
$\pm 2\theta$	$2\phi(x, 2\theta)_{T_4}$	I_{T_1, T_2} $\otimes S_{T_3, T_4} \otimes I_{T_5, T_6}$
$\pm 3\theta$	$2\phi(x, 3\theta)_{T_4}$	I_{T_1, T_2} $\otimes S_{T_3, T_4} \otimes S_{T_5, T_6}$
$\pm 4\theta$	$2\phi(x, 4\theta)_{T_5}$	I_{T_1, T_2} $\otimes I_{T_3, T_4} \otimes S_{T_5, T_6}$
$\pm 5\theta$	$2\phi(x, 5\theta)_{T_5}$	S_{T_1, T_2} $\otimes I_{T_3, T_4} \otimes S_{T_5, T_6}$
$\pm 6\theta$	$2\phi(x, 6\theta)_{T_5}$	I_{T_1, T_2} $\otimes S_{T_3, T_4} \otimes S_{T_5, T_6}$
$\pm 7\theta$	$2\phi(x, 7\theta)_{T_5}$	S_{T_1, T_2} $\otimes S_{T_3, T_4} \otimes S_{T_5, T_6}$

as

$$\begin{aligned}
|\Psi\rangle_2 = & (\beta_1|HV\rangle_{AB}|\phi\rangle_{CD}|\phi\rangle_{EF} \\
& \otimes |C_2\rangle|T_1T_4\rangle|T_5T_8\rangle \\
& + \beta_2|VH\rangle_{AB}|\phi\rangle_{CD}|\phi\rangle_{EF} \\
& \otimes |C_1\rangle|T_2T_3\rangle|T_6T_7\rangle)|\alpha_6\rangle \\
& + \beta_1|HV\rangle_{AB}|\phi\rangle_{CD}|\phi\rangle_{EF} \\
& \otimes |C_2\rangle|T_2T_3\rangle|T_6T_7\rangle|\alpha_6e^{2i\theta}\rangle \\
& + \beta_2|VH\rangle_{AB}|\phi\rangle_{CD}|\phi\rangle_{EF} \\
& \otimes |C_1\rangle|T_1T_4\rangle|T_5T_8\rangle|\alpha_6e^{-2i\theta}\rangle. \quad (23)
\end{aligned}$$

If no phase shift is induced in the coherent state $|\alpha_6\rangle$, there is nothing to do. However, if a phase shift of $\pm 2\theta$ is induced, a feed-forward $\phi(x, 2\theta)$ operation is applied on path T_1 , followed by four SWAP gates applied on some paths (T_1, T_2), (T_3, T_4), (T_5, T_6) and (T_7, T_8). Then, the finally state is given by

$$\begin{aligned}
|\Psi\rangle'_2 = & \beta_1|HV\rangle_{AB}|\phi\rangle_{CD}|\phi\rangle_{EF}|C_2\rangle|T_1T_4\rangle|T_5T_8\rangle \\
& + \beta_2|VH\rangle_{AB}|\phi\rangle_{CD}|\phi\rangle_{EF}|C_1\rangle|T_2T_3\rangle|T_6T_7\rangle. \quad (24)
\end{aligned}$$

Thirdly, two SWAP gates are executed on the target photons CE on two paths $|T_2T_6\rangle$ and the

target photons DF on two paths $|T_3T_7\rangle$, respectively, and the quantum state is evolved into

$$|\Psi\rangle_3 = \beta_1|\bar{0}\rangle_{AB}|\phi\rangle_{CD}|\phi\rangle_{EF}|C_2\rangle|T_1T_4\rangle|T_5T_8\rangle + \beta_2|\bar{1}\rangle_{AB}|\phi\rangle_{CD}|\phi\rangle_{EF}|C_1\rangle|T_2T_3\rangle|T_6T_7\rangle, \quad (25)$$

where

$$\overline{|\phi\rangle_{CD}|\phi\rangle_{EF}} = (\gamma_1|\bar{0}\rangle + \gamma_2|\bar{1}\rangle)_{CD} \otimes (\delta_1|\bar{0}\rangle + \delta_2|\bar{1}\rangle)_{EF}. \quad (26)$$

Finally, the control photons AB traverse PBS_2 and the target photons CD and EF traverse two path couplers in Figure 1b to simplify the circuits, respectively, and the desirous state is obtained

$$|\Psi\rangle_4 = (\beta_1|\bar{0}\rangle_{AB}|\phi\rangle_{CD}|\phi\rangle_{EF} + \beta_2|\bar{1}\rangle_{AB}\overline{|\phi\rangle_{CD}|\phi\rangle_{EF}}) \otimes |C_1C_2\rangle|T_1T_4\rangle|T_5T_8\rangle. \quad (27)$$

Apparently, based on Eq. (27), the three-logic-qubit Fredkin gate encoding with six photons ABCDEF in DFS is fulfilled perfectly with the success probability close to 1, by performing appropriate feed-forward operations in Tables 1 and 4, where the Fredkin gate swaps the states of the target photons CD and EF if and only if the control photons AB is in the state $|\bar{1}\rangle_{AB}$, and has no change otherwise.

4 Success probabilities and fidelities of quantum gates regard to photon loss

In view of cross-Kerr nonlinearities, the principles of three schemes for CNOT, Toffoli, and Fredkin gates in DFS to overcome decoherence, are discussed in detail in Sec. 3. Besides, the path couplers of three quantum logical gates are employed to simplify the complexity of quantum circuits and halve the number of the paths of the photons without destroying the polarization information of these photons. As the function conforming to $f(x, \alpha \cos \theta) = (2\pi)^{-1/4} \exp[-(x - 2\alpha \cos \theta)^2/4]$ cannot differentiate phase shift $\pm\theta$ of the coherent states, the X-homodyne measurement can obtain four scenarios of phase shifts, i.e., $0, \pm 2\theta, \pm 3\theta, \pm 5\theta$ from the corresponding coherent states $|\alpha_1\rangle, |\alpha_2\rangle, |\alpha_3\rangle$, and $|\alpha_4\rangle$ for implementation of the path couplers, two-logic-qubit CNOT gate, and three-logic-qubit Toffoli gate. It can also distinguish eight scenarios of phase

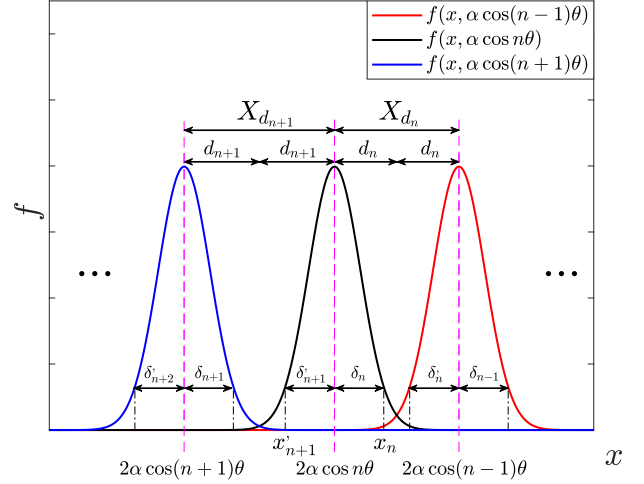


Figure 5: Gaussian function curves $f(x, \alpha \cos(n-1)\theta)$ (red line), $f(x, \alpha \cos n\theta)$ (black line), and $f(x, \alpha \cos(n+1)\theta)$ (blue line). The symbol X_{d_n} stands for the distance between the peaks of Gaussian function curves $f(x, \alpha \cos(n-1)\theta)$ and $f(x, \alpha \cos n\theta)$. The symbol $X_{d_{n+1}}$ represents the distance between the peaks of Gaussian function curves $f(x, \alpha \cos n\theta)$ and $f(x, \alpha \cos(n+1)\theta)$. $X_{d_n} = 2d_n$ and $X_{d_{n+1}} = 2d_{n+1}$. x_n and x'_{n+1} are measurement outcomes of X Homodyne measurement. δ_n (δ'_{n+1}) is the distance between measurement outcomes x_n (x'_{n+1}) and the peak point ($x = 2\alpha \cos n\theta$) of the Gaussian function curve $f(x, \alpha \cos n\theta)$.

shifts, i.e., $0, \pm\theta, \pm 2\theta, \dots, \pm 7\theta$ from the coherent states $|\alpha_5\rangle$ and two scenarios of phase shifts, i.e., $0, \pm 2\theta$ from the coherent state $|\alpha_6\rangle$ for implementation of the three-logic-qubit Fredkin gate. Next, we analyze the success probabilities and fidelities of our quantum gates.

4.1 Success probabilities of quantum gates regard to photon loss

The success probabilities P_{suc} of the our protocols relies on the precise measurement of the X-quadrature homodyne. The Gaussian function curves $f(x, \alpha \cos(n-1)\theta)$ and $f(x, \alpha \cos n\theta)$ partially overlap, resulting in errors between phase shifts $(n-1)\theta$ and $n\theta$ shown in Figure 5. The symbol X_{d_n} stands for the distance between the peaks of Gaussian function curves $f(x, \alpha \cos(n-1)\theta)$ and $f(x, \alpha \cos n\theta)$. Besides, the symbol $X_{d_{n+1}}$ represents the distance between the peaks of Gaussian function curves $f(x, \alpha \cos(n)\theta)$ and $f(x, \alpha \cos(n+1)\theta)$. The photon loss of the probe coherent field in the nonlinear Kerr medium leads to $\alpha \rightarrow A\alpha$, where γ is the decay constant and $A = e^{-\frac{1}{2}\gamma t}$ is the coherence parameter reducing

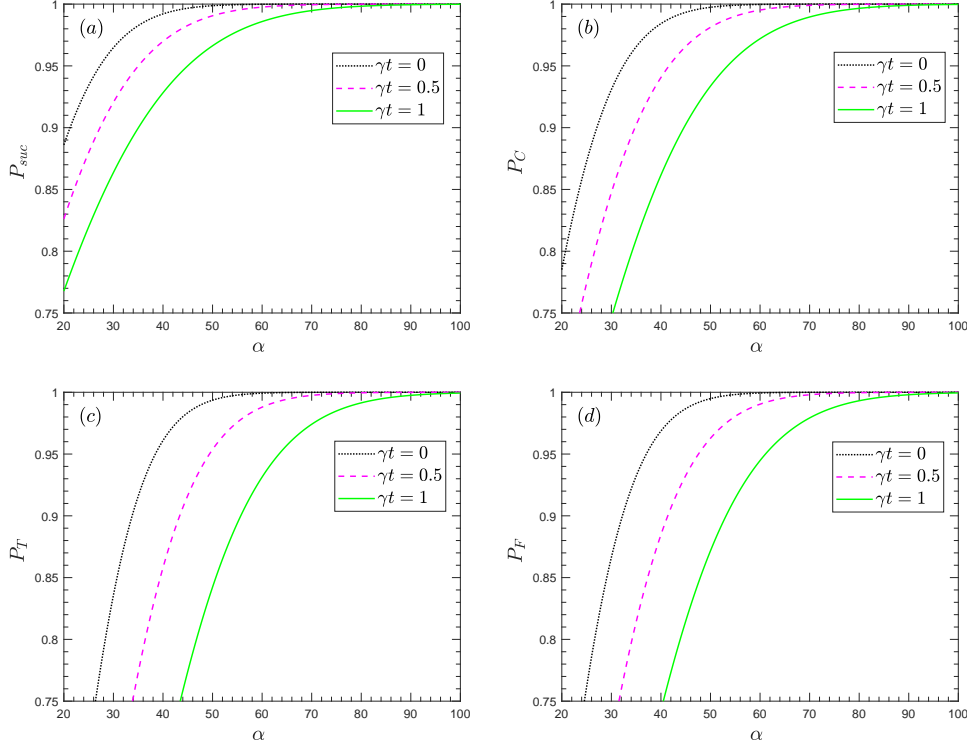


Figure 6: (a) The success probability $P_{suc}(\alpha, \gamma t)$ of the X-homodyne measurement of the path coupler vs the amplitude α for the fixed dimensionless parameters $\theta = 0.35$ [60] with the various conditions $\gamma t = 0$ (black dotted line), $\gamma t = 0.5$ (purple dashed line), and $\gamma t = 1$ (green line), respectively. (b)-(d) show the corresponding success probabilities of our logic gates with the same condition as (a).

the amplitude of coherent state and making the original pure state to evolve into a mixed state of the photons. Considering the photon dissipation of the coherent state, the success probability P_{suc} of the path coupler with once interaction can be calculated by [31]

$$P_{suc}(\alpha, \theta, \gamma t) = 1 - \frac{1}{2} \operatorname{erfc}\left[\frac{A\alpha(1 - \cos \theta)}{\sqrt{2}}\right], \quad (28)$$

where $\operatorname{erfc}(x)$ is a Gauss complementary error function. The factors that determine the success probability P_{suc} include α , θ , and γt . Considering the cascade effects of the homodyne detection, the application of twice, five times, and four times X-homodyne measurements to realize the CNOT gate, Toffoli gate, and Fredkin gate, respectively, so the success probabilities of the CNOT gate (P_C), Toffoli gate (P_T), and Fredkin gate (P_F) can be calculated as P_{suc}^2 , P_{suc}^5 , and P_{suc}^4 ignoring the imperfect influence of linear optical elements. Firstly, we discuss the success probability $P_{suc}(\alpha, \gamma t)$ of the precise measurement of the X-homodyne detectors vs amplitude α with different conditions $\gamma t = 0$, $\gamma t = 0.5$,

and $\gamma t = 1$ for fixed the parameters $\theta = 0.35$ [60], depicted in Figure 6a. The success probability P_C , P_T , and P_F of the CNOT, Toffoli, and Fredkin gates, with the same condition are shown in Figs. 6 (b)-(d), respectively. If the amplitude α of the coherent state increases and dissipation coefficient γt decreases, the success probabilities of our schemes increase. By calculation with the different parameters of Ref. [29, 31], six sets of data $P_{suc}(\alpha, \gamma t)$ are obtained, e.g., $P_{suc}(40, 1) = 0.9282$, $P_{suc}(50, 1) = 0.9662$, $P_{suc}(40, 0.5) = 0.9698$, $P_{suc}(50, 0.5) = 0.9906$, $P_{suc}(40, 0) = 0.9921$, and $P_{suc}(50, 0) = 0.9987$. Based on the analyses above, the nearly deterministic quantum logical gates, i.e., CNOT, Toffoli, and Fredkin gates in DFS, can be achieved.

Above discussion about the success probabilities of our protocols, we only investigate the main factor α . In view of the strength of natural cross-Kerr nonlinearity [61] is so small that it cannot provide effective interactions between photons, which leads to increasing the difficulty in distinguishing two overlapping coherent states and decreasing the success probabilities of the path cou-

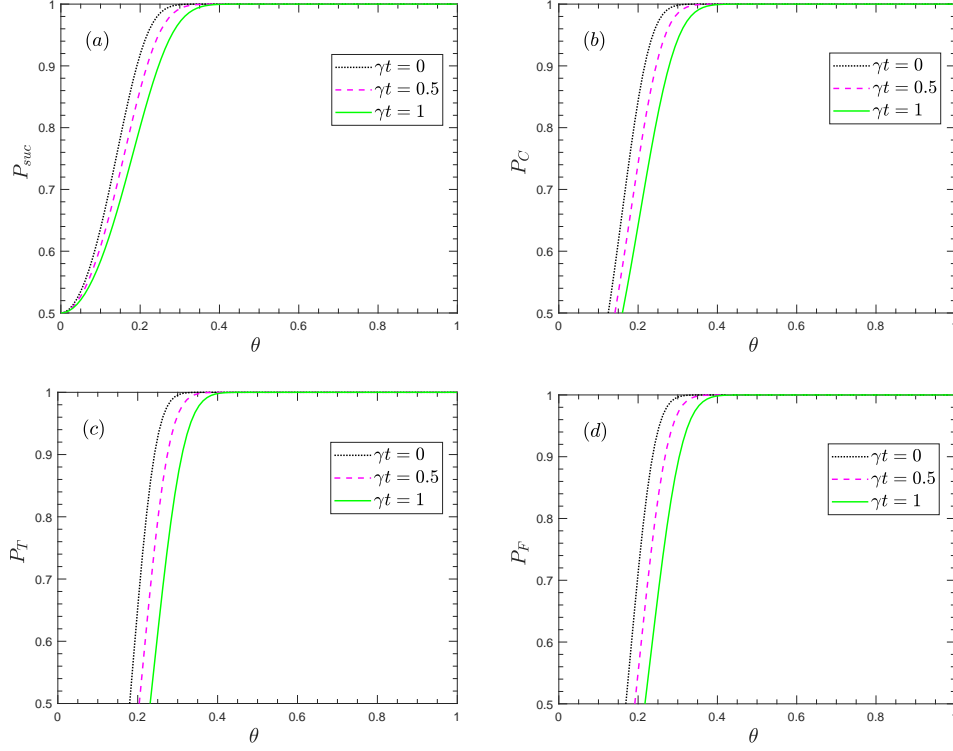


Figure 7: (a) The success probability $P_{suc}(\theta, \gamma t)$ of the X-homodyne measurement of the path coupler vs the phase shift θ for the fixed amplitude $\alpha = 70$ with the various conditions $\gamma t = 0$ (black dotted line), $\gamma t = 0.5$ (purple dashed line), and $\gamma t = 1$ (green line), respectively. (b)-(d) show the corresponding success probabilities of our logic gates with the same condition as (a).

pler and three gates. Fortunately, various physical systems or synthetic media, such as negative-index metamaterials [62], a superconducting artificial atom [60], and a three-dimensional quantum electrodynamic architectures [63, 64], have been explored to achieve stronger cross-Kerr nonlinearities. The paper in Ref. [62] mentioned that the Kerr nonlinearity χ (10^{-4}) can be achieved between the surface polaritons and the mutual phase shift was approximate π . Another paper in Ref. [60] demonstrated the cross-Kerr phase shift up to 0.35 ($\theta \simeq 20^\circ$) based on per photon with the coherent microwave field at the single-photon level. Ref. [64] mentioned they designed phase shift large enough ($\theta > 30^\circ \approx 0.52$). Figure 7a illustrates the success probability $P_{suc}(\theta, \gamma t)$ of the X-homodyne measurement of the path coupler vs the phase shift θ with the different conditions $\gamma t = 0$, $\gamma t = 0.5$, and $\gamma t = 1$ for fixed the parameters $\alpha = 70$. If the phase shift θ increases and dissipation coefficient γt decreases, the success probabilities of our schemes increase. Figs. 7 (b)-(d) show the corresponding success probabilities of our logic gates. By calculation

with the different parameters of Ref. [60, 62–64], six sets of data $P_{suc}(\theta, \gamma t)$ are obtained, e.g., $P_{suc}(0.35, 1) = 0.9801$, $P_{suc}(0.52, 1) = 1$, $P_{suc}(0.35, 0.5) = 0.9981$, $P_{suc}(0.52, 0.5) = 1$, $P_{suc}(0.35, 0) = 1$, and $P_{suc}(0.52, 0) = 1$. Similarly, the success probabilities of three logical gates in DFS are close to 1.

Besides, phase shift θ can be increased by prolonging the interaction time between photons and coherent state [65–68], as well as measurement-based methods [69–71] and quadrature squeezing operations [72] to achieve large phase shift. By employing a two-level atom in a one-sided cavity and the displacements-controlled photon number resolving (PNR) detector, accomplished phase shift π can be obtained [73]. Thus, in the case $\alpha\theta^2 \gg 1$, one can realize the deterministic distinguishability between the shifted and non-shifted phases in the coherent state, where the cross-Kerr nonlinearities $\theta \ll 1$ with a sufficiently large amplitude of the coherent states can be applicable. Furthermore, two coherent states can be discriminated to lower the error probability, resorting to a homodyne detector and a PNR

detector applying the postselection strategy [74]. Therefore, we set up the CNOT, Toffoli and Fredkin gates in DFS based on Kerr effects, which can overcome and alleviate the disadvantageous factors, ultimately reducing the error probabilities.

4.2 Fidelities of our quantum gates regard to photon loss

The coupling between the coherent state and environment causes the loss of photons of the coherent state, so we consider the influence of photon loss on fidelity. The decoherence effects for the coherent state described by the standard master equation

$$\begin{aligned}\frac{\partial \rho}{\partial t} &= \hat{J}\rho + \hat{L}\rho, \quad \hat{J}\rho = \gamma a \rho a^\dagger, \\ \hat{L}\rho &= -\frac{\gamma}{2} a a^\dagger \rho + \rho a a^\dagger,\end{aligned}\quad (29)$$

where a and a^\dagger are the annihilation and creation operators of the coherent state, respectively. ρ denotes the density matrix of the system. The formal solution of the master Eq. (29) can be written as $\rho(t) = e^{(\hat{J}+\hat{L})t}\rho(0)$ and t is the interaction time. The evolution of the hybrid system caused by nonlinear interactions between the photons and the coherent states could be described by a unitary evolution equation $\tilde{U}(t)\rho(0) = U(t)\rho(0)U^\dagger(t)$. Assumed that the interaction time t is defined on the temporal interval $[a, b]$ and is divided into N parts $a = x_0 < x_1 < x_2 < \dots < x_N = b$ ($N \approx \infty$), setting $\Delta x_N = x_N - x_{N-1}$, the decoherence process \tilde{D} occurs for a short time Δx_N and the unitary evolution operator \tilde{U} occurs for next temporal interval Δx_{N+1} ($N = 1, 2, 3, \dots$). After the finite temporal interval t , the system would evolve as $\rho(t) = [\tilde{D}(\Delta t)\tilde{U}(\Delta t)]^N \rho(0)$ [75].

As four scenarios of phase shifts, i.e., $0, \pm 2\theta, \pm 3\theta, \pm 5\theta$ from the corresponding coherent states $|\alpha_1\rangle, |\alpha_2\rangle, |\alpha_3\rangle$, and $|\alpha_4\rangle$ for implementation of the path coupler, two-logic-qubit CNOT gate, and three-logic-qubit Toffoli gate, and eight scenarios of phase shifts, i.e., $0, \pm\theta, \pm 2\theta, \dots, \pm 7\theta$ from the coherent states $|\alpha_5\rangle$ for implementation

of the three-logic-qubit Fredkin gate can be obtained by the X-homodyne measurements. We take the fidelity F_C of the two-logic-qubit CNOT gate as an example to denote in detail. The initial state is $|\Omega\rangle$ in Eq. (12), the density matrix of the system is $\rho(0) = |\Omega\rangle\langle\Omega|$. In the realm of Kerr media, the system is successively affected by $\tilde{U}(\Delta t)$ as

$$\begin{aligned}\tilde{U}(\Delta t)\rho(0) &= U(\Delta t)|\Omega\rangle\langle\Omega|U^\dagger(\Delta t) \\ &= \sum_{k,l=-5}^5 |\phi_k\rangle\langle\phi_l| \otimes |\alpha e^{i\frac{k\theta}{N}}\rangle\langle\alpha e^{i\frac{l\theta}{N}}|, \\ &k, l \in \{0, \pm 2, \pm 3, \pm 5\}.\end{aligned}\quad (30)$$

Here,

$$\begin{aligned}|\phi_0\rangle &= \beta_1|\bar{0}\rangle_{AB}|\phi\rangle_{CD}|C_2\rangle|T_1T_4\rangle \\ &\quad + \beta_2|\bar{1}\rangle_{AB}|\phi\rangle_{CD}|C_1\rangle|T_2T_3\rangle, \\ |\phi_2\rangle &= \beta_1|\bar{0}\rangle_{AB}|\phi\rangle_{CD}|C_2\rangle|T_1T_3\rangle, \\ |\phi_{-2}\rangle &= \beta_2|\bar{1}\rangle_{AB}|\phi\rangle_{CD}|C_1\rangle|T_2T_4\rangle, \\ |\phi_3\rangle &= \beta_1|\bar{0}\rangle_{AB}|\phi\rangle_{CD}|C_2\rangle|T_2T_4\rangle, \\ |\phi_{-3}\rangle &= \beta_2|\bar{1}\rangle_{AB}|\phi\rangle_{CD}|C_1\rangle|T_1T_3\rangle, \\ |\phi_5\rangle &= \beta_1|\bar{0}\rangle_{AB}|\phi\rangle_{CD}|C_2\rangle|T_2T_3\rangle, \\ |\phi_{-5}\rangle &= \beta_2|\bar{1}\rangle_{AB}|\phi\rangle_{CD}|C_1\rangle|T_1T_4\rangle.\end{aligned}\quad (31)$$

and $\tilde{D}(\Delta t)$ as

$$\begin{aligned}\tilde{D}(\Delta t)\tilde{U}(\Delta t)\rho(0) &= \sum_{k,l=-5}^5 \exp\{\alpha^2(1 - e^{-\frac{\gamma}{N}})[e^{i(k-l)\frac{\theta}{N}} - 1]\} \\ &\times |\phi_k\rangle\langle\phi_l| \otimes |e^{-\frac{\gamma t}{2N}}\alpha e^{i\frac{k\theta}{N}}\rangle\langle e^{-\frac{\gamma t}{2N}}\alpha e^{i\frac{l\theta}{N}}|.\end{aligned}\quad (32)$$

Consequently, the system is changed into

$$\begin{aligned}\rho(t) &= [\tilde{D}(\Delta t)\tilde{U}(\Delta t)]^N \rho(0) \\ &= \sum_{k,l=-5}^5 e^{B_{kl}} |\phi_k\rangle\langle\phi_l| \otimes |Ae^{ik\theta}\rangle\langle Ae^{il\theta}|,\end{aligned}\quad (33)$$

where $B_{kl} = \alpha^2(1 - A^{\frac{2}{N}}) \sum_{n=1}^N A^{\frac{2(n-1)}{N}} [e^{i(k-l)\frac{n\theta}{N}} - 1]$. After performing X measurement on the dissipated coherent state, the resulting state can be obtained as follows

$$\langle x|\rho(t)|x\rangle = \sum_{k,l=-5}^5 C_{kl} |\phi_k\rangle\langle\phi_l| \times f(x, k\theta) f(x, l\theta) e^{i[\delta_{kl} + \varphi(x, k\theta) - \varphi(x, l\theta)]}, \quad (34)$$

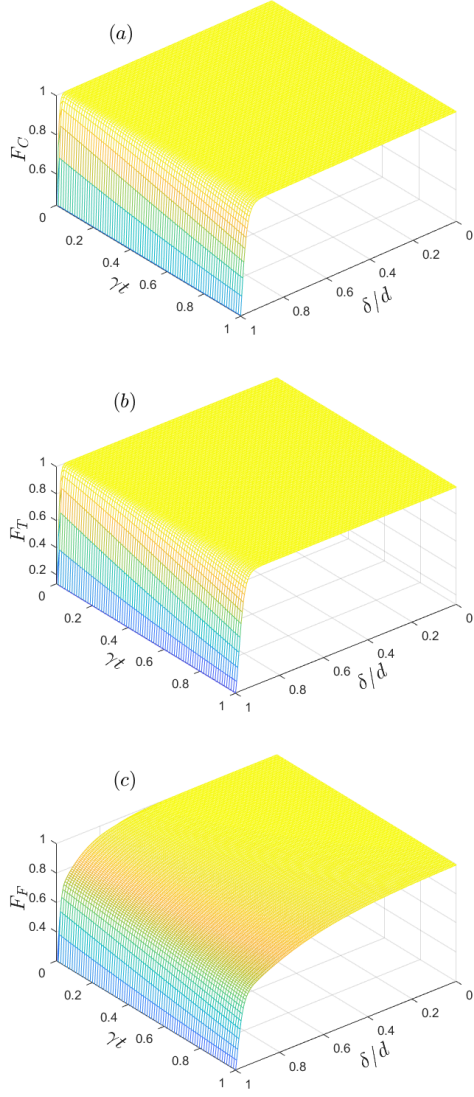


Figure 8: (a) The fidelity F_C of CNOT gate (b) the fidelity F_T of the Toffoli gate (c) the fidelity F_F of the Fredkin gate vs the amplitude of the coherent state α and the dissipation coefficient γt for the parameters $N = 200$, $\theta = 20^\circ \approx 0.35$ [60].

where $C_{kl} = e^{\text{Re}(B_{kl})}$, $\delta_{kl} = \text{Im}(B_{kl})$, the function $f(x, n\theta) = (2\pi)^{-\frac{1}{4}} \exp[-(x - 2A\alpha \cos \theta)^2/4]$, and $\varphi(x, n\theta) = (x - 2A\alpha \cos n\theta)A\alpha \sin n\theta$ ($n = 0, \pm 2, \pm 3, \pm 5$).

Based on the fidelity formula $F = \langle \Psi | \rho_{out} | \Psi \rangle_{ideal}$ [72, 76] determined by the real output state and the ideal one ($|\Omega\rangle_3, |\Phi\rangle_5$, or $|\Psi\rangle_4$), the fidelities of three gates vs the dissipation term γt as well as α with the parameters set as $N = 200$ and $\theta = 0.35$ [60] are plotted in Figure 8. X_{d_n} is the distance between the highest points of two adjacent Gaussian curves ($2d_n = X_{d_n}$), which increases leading to the reduction of overlap between the two Gauss func-

tions. δ_n is the distance between measurement outcomes x_n and the peak point ($x = 2\alpha \cos n\theta$) of the Gaussian function curve $f(x, \alpha \cos n\theta)$. It can be seen that the fidelities F_C , F_T , and F_F decrease with the increasing δ/d and the reducing γt . By calculation with the different parameters of Ref. [29, 31], four sets of data $F(\delta/d, \gamma t)$ are obtained, e.g., $F_C(0.8, 0) = 1$, $F_C(0.8, 1) = 1$, $F_C(0.95, 0) = 0.9997$, $F_C(0.95, 1) = 0.9631$; $F_T(0.8, 0) = 1$, $F_T(0.8, 1) = 1$, $F_T(0.95, 0) = 0.9994$, $F_T(0.95, 1) = 0.9275$; $F_F(0.6, 0) = 0.9912$, $F_F(0.6, 1) = 0.9193$, $F_F(0.8, 0) = 0.914$, $F_F(0.8, 1) = 0.8268$. Based on the analyses above, the high fidelities of quantum logic gates in DFS can be achieved even though under the decoherence environment.

5 SUMMARY

In summary, with the help of the cross-Kerr nonlinearities, we propose the effectuation of the nearly deterministic two-logic-qubit CNOT gate, three-logic-qubit Toffoli gate, and Fredkin gate encoded on polarization degrees of freedom of photon systems due to the significant features, e.g., the low-decoherence character, flexible single-qubit manipulation, and ultra-fast transmission. Moreover, the SWAP gates and the path couplers are innovated for implementing three logical gates. The SWAP gate, which serves to swap the polarized states of two photons as well as two paths of a single photon, is set up with simple linear-optics elements, so its success probability is 1, The path coupler with the probability near close to 1 is utilized to combine two paths of the photon to the one by available single-qubit operations and mature measurement methods, which halves the number of the paths of the photon and greatly simplifies the quantum circuits. Therefore, these three logical gates require neither complicated quantum computational circuits nor auxiliary photons (or entangled states). Further, the success probabilities of three logical gates are approximate 1 by performing the corresponding classical feed-forward operations based on the different measuring results of the X-homodyne detectors to be aimed at the coherent states. Eventually, their fidelities are robust against the photon loss with the current technology. The proposed schemes play positive roles in the future development of QIP owing to the

robust feature by resisting the influence of decoherence effect in DFS.

Acknowledgments

This work was supported in part by the Natural Science Foundation of China under Contract 61901420; in part by Fundamental Research Program of Shanxi Province under Contract 20230302121116.

Disclosures

The authors declare that there are no conflicts of interest related to this article. Data Availability.

Data Availability

Data underlying the results presented in this paper are not publicly available at this time but may be obtained from the authors upon reasonable request.

References

- [1] Lov K. Grover Michael A. Nielsen, Isaac Chuang. “Quantum computation and quantum information”. *Am. J. Phys.* **70**, 558–559 (2002).
- [2] Mingxia Huo and Ying Li. “Error-resilient Monte Carlo quantum simulation of imaginary time”. *Quantum* **7**, 916 (2023).
- [3] Masahito Hayashi and Yuxiang Yang. “Efficient algorithms for quantum information bottleneck”. *Quantum* **7**, 936 (2023).
- [4] XiuZhe Luo, JinGuo Liu, Pan Zhang, and Lei Wang. “Yao.jl: Extensible, Efficient Framework for Quantum Algorithm Design”. *Quantum* **4**, 341 (2020).
- [5] Xin Wang, Zhixin Song, and Youle Wang. “Variational Quantum Singular Value Decomposition”. *Quantum* **5**, 483 (2021).
- [6] G. L. Long and X. S. Liu. “Theoretically efficient high-capacity quantum-key-distribution scheme”. *Phys. Rev. A* **65**, 032302 (2002).
- [7] Wei Zhang, Dong Sheng Ding, Yu Bo Sheng, Lan Zhou, Bao Sen Shi, and Guang Can Guo. “Quantum secure direct communication with quantum memory”. *Phys. Rev. Lett.* **118**, 220501 (2017).
- [8] Feng Zhu, Wei Zhang, Yu Bo Sheng, and Yi Dong Huang. “Experimental long-distance quantum secure direct communication”. *Sci. Bull.* **62**, 1519–1524 (2017).
- [9] Fang-Fang Du, Yong-Ting Liu, Zhen-Rong Shi, Yu-Xi Liang, Jun Tang, and Jun Liu. “Efficient hyperentanglement purification for three-photon systems with the fidelity-robust quantum gates and hyperentanglement link”. *Opt. Express* **27**, 27046–27061 (2019).
- [10] Tao Li and Gui Lu Long. “Quantum secure direct communication based on single-photon bell-state measurement”. *New J. Phys.* **22**, 063017 (2020).
- [11] Zixin Huang, Peter P. Rohde, Dominic W. Berry, Pieter Kok, Jonathan P. Dowling, and Cosmo Lupo. “Photonic quantum data locking”. *Quantum* **5**, 447 (2021).
- [12] Chuan Wang. “Quantum secure direct communication: Intersection of communication and cryptography”. *Fundam. Res.* **1**, 91–92 (2021).
- [13] Zhantong Qi, Yuanhua Li, Yiwen Huang, Juan Feng, Yuanlin Zheng, and Xianfeng Chen. “A 15-user quantum secure direct communication network”. *Light Sci. Appl.* **10**, 183 (2021).
- [14] G. L. Long and H. Zhang. “Drastic increase of channel capacity in quantum secure direct communication using masking”. *Sci. Bull.* **66**, 1267–1269 (2021).
- [15] Yu Bo Sheng, Lan Zhou, and Gui Lu Long. “One-step quantum secure direct communication”. *Sci. Bull.* **67**, 367–374 (2022).
- [16] Yue Ru Zhou, Qing Feng Zhang, Fei Fei Liu, Yu Hong Han, Yong Pan Gao, Ling Fan, Ru Zhang, and Cong Cao. “Controllable nonreciprocal phonon laser in a hybrid photonic molecule based on directional quantum squeezing”. *Opt. Express* **32**, 2786–2803 (2024).
- [17] Peng Zhao, Meng Ying Yang, Sha Zhu, Lan Zhou, Wei Zhong, Ming Ming Du, and Yu Bo Sheng. “Generation of hyperentangled state encoded in three degrees of freedom”. *Sci. China Phys. Mech.* **66**, 100311 (2023).
- [18] Yun Feng Guo, Wei Zhong, Lan Zhou, and

- Yu Bo Sheng. “Supersensitivity of kerr phase estimation with two-mode squeezed vacuum states”. *Phys. Rev. A* **105**, 032609 (2022).
- [19] Cong Cao, Yu-Hong Han, Li Zhang, Ling Fan, Yu-Wen Duan, and Ru Zhang. “High-fidelity universal quantum controlled gates on electron-spin qubits in quantum dots inside single-sided optical microcavities”. *Adv. Quantum Technol.* **2**, 1900081 (2019).
- [20] Cong Cao, Li Zhang, Yu Hong Han, Pan Pan Yin, Ling Fan, Yu Wen Duan, and Ru Zhang. “Complete and faithful hyperentangled-bell-state analysis of photon systems using a failure-heralded and fidelity-robust quantum gate”. *Opt. Express* **28**, 2857–2872 (2020).
- [21] Yi Ming Wu, Gang Fan, and Fang Fang Du. “Error-detected three-photon hyperparallel toffoli gate with state-selective reflection”. *Front. Phys.* **17**, 51502 (2022).
- [22] Xiu Yu Zhang, Cong Cao, Yong Pan Gao, Ling Fan, Ru Zhang, and Chuan Wang. “Generation and manipulation of phonon lasing in a two-drive cavity magnomechanical system”. *New J. Phys.* **25**, 053039 (2023).
- [23] Wen Qiang Liu and Hai Rui Wei. “Optimal synthesis of the fredkin gate in a multilevel system”. *New J. Phys.* **22**, 063026 (2020).
- [24] Wen Qiang Liu, Hai Rui Wei, and Leong Chuan Kwek. “Low-cost fredkin gate with auxiliary space”. *Phys. Rev. Appl.* **14**, 054057 (2020).
- [25] Jaromír Fiurášek. “Linear optical fredkin gate based on partial-swap gate”. *Phys. Rev. A* **78**, 032317 (2008).
- [26] Fabio Dell’Anno, Silvio De Siena, and Fabrizio Illuminati. “Multiphoton quantum optics and quantum state engineering”. *Phys. Rep.* **428**, 53–168 (2006).
- [27] Gui-Long Jiang, Jun-Bin Yuan, Wen-Qiang Liu, and Hai-Rui Wei. “Efficient and deterministic high-dimensional controlled-swap gates on hybrid linear optical systems with high fidelity”. *Phys. Rev. Appl.* **21**, 014001 (2024).
- [28] Kae Nemoto and W. J. Munro. “Nearly deterministic linear optical controlled-not gate”. *Phys. Rev. Lett.* **93**, 250502 (2004).
- [29] Qing Lin and Jian Li. “Quantum control gates with weak cross-kerr nonlinearity”. *Phys. Rev. A* **79**, 022301 (2009).
- [30] Qing Lin and Bing He. “Single-photon logic gates using minimal resources”. *Phys. Rev. A* **80**, 042310 (2009).
- [31] Li Dong, Sen Lin Wang, Cen Cui, Xue Geng, Qing Yang Li, Hai Kuan Dong, Xiao Ming Xiu, and Ya Jun Gao. “Polarization toffoli gate assisted by multiple degrees of freedom”. *Opt. Lett.* **43**, 4635–4638 (2018).
- [32] Fang Fang Du, Gang Fan, Xue Mei Ren, and Ming Ma. “Deterministic hyperparallel control gates with weak kerr effects”. *Adv. Quantum Technol.* **6**, 2300201 (2023).
- [33] Hai Rui Wei and Fu Guo Deng. “Compact quantum gates on electron-spin qubits assisted by diamond nitrogen-vacancy centers inside cavities”. *Phys. Rev. A* **88**, 042323 (2013).
- [34] Qing Ai, Peng-Bo Li, Wei Qin, Jie-Xing Zhao, C. P. Sun, and Franco Nori. “The nv metamaterial: Tunable quantum hyperbolic metamaterial using nitrogen vacancy centers in diamond”. *Phys. Rev. B* **104**, 014109 (2021).
- [35] Fang Fang Du, Xue Mei Ren, Ming Ma, and Gang Fan. “Qudit-based high-dimensional controlled-not gate”. *Opt. Lett.* **49**, 1229 (2024).
- [36] Hai Rui Wei and Fu Guo Deng. “Universal quantum gates on electron-spin qubits with quantum dots inside single-side optical microcavities”. *Opt. Express* **22**, 593–607 (2014).
- [37] Hai Rui Wei, Yan Bei Zheng, Ming Hua, and Guo Fu Xu. “Robust-fidelity hyperparallel controlled-phase-flip gate through microcavities”. *Appl. Phys. Express* **13**, 082007 (2020).
- [38] Yu Hong Han, Cong Cao, Ling Fan, and Ru Zhang. “Heralded high-fidelity quantum hyper-cnot gates assisted by charged quantum dots inside single-sided optical microcavities”. *Opt. Express* **29**, 20045–20062 (2021).
- [39] Guo Zhu Song, Jin Liang Guo, Qian Liu, Hai Rui Wei, and Gui Lu Long. “Heralded quantum gates for hybrid systems via waveguide-mediated photon scattering”. *Phys. Rev. A* **104**, 012608 (2021).
- [40] Tao Li, Adam Miranowicz, Ke Yu Xia, and

- Franco Nori. “Resource-efficient analyzer of bell and greenberger-horne-zeilinger states of multiphoton systems”. *Phys. Rev. A* **100**, 052302 (2019).
- [41] Guo Zhu Song, Ming Jie Tao, Jing Qiu, and Hai Rui Wei. “Quantum entanglement creation based on quantum scattering in one-dimensional waveguides”. *Phys. Rev. A* **106**, 032416 (2022).
- [42] Fang Fang Du and Zhen Rong Shi. “Robust hybrid hyper-controlled-not gates assisted by an input-output process of low-q cavities”. *Opt. Express* **27**, 17493–17506 (2019).
- [43] Fang Fang Du, Yi Ming Wu, and Gang Fan. “Refined quantum gates for λ -type atom-photon hybrid systems”. *Adv. Quantum Technol.* **6**, 2300090 (2023).
- [44] Frank Arute, Kunal Arya, Ryan Babush, Dave Bacon, Joseph C Bardin, Rami Barends, Rupak Biswas, Sergio Boixo, Fernando GSL Brandao, David A Buell, et al. “Quantum supremacy using a programmable superconducting processor”. *Nature* **574**, 505–510 (2019).
- [45] Lu Ming Duan and Guang Can Guo. “Preserving coherence in quantum computation by pairing quantum bits”. *Phys. Rev. Lett.* **79**, 1953–1956 (1997).
- [46] Hua Wei, Wan Li Yang, Zhi Jiao Deng, and Mang Feng. “Many-qubit network employing cavity qed in a decoherence-free subspace”. *Phys. Rev. A* **78**, 014304 (2008).
- [47] Z. J. Deng, M. Feng, and K. L. Gao. “Preparation of entangled states of four remote atomic qubits in decoherence-free subspace”. *Phys. Rev. A* **75**, 024302 (2007).
- [48] Lei Chen, Xiao Ming Xiu, Li Dong, Shou Zhang, Shi Lei Su, Shu Chen, and Er Jun Liang. “Conversion of knill–laflamme–milburn entanglement to greenberger–horne–zeilinger entanglement in decoherence-free subspace”. *Ann. Phys.* **534**, 2100365 (2022).
- [49] Lei Chen, Xiao Ming Xiu, Li Dong, Nan Nan Liu, Cai Peng Shen, Shou Zhang, Shu Chen, and Shi Lei Su. “Direct conversion of greenberger–horne–zeilinger state to knill–laflamme–milburn state in decoherence-free subspace”. *Opt. Lett.* **47**, 2262–2265 (2022).
- [50] Fang Fang Du, Xue Mei Ren, Zhi Guo Fan, Ling Hui Li, Xin Shan Du, Ming Ma, Gang Fan, and Jing Guo. “Decoherence-free-subspace-based deterministic conversions for entangled states with heralded robust-fidelity quantum gates”. *Opt. Express* **32**, 1686 (2024).
- [51] Yi Fan Qiao, Jia Qiang Chen, Xing Liang Dong, Bo Long Wang, Xin Lei Hei, Cai Peng Shen, Yuan Zhou, and Peng Bo Li. “Generation of greenberger-horne-zeilinger states for silicon-vacancy centers using a decoherence-free subspace”. *Phys. Rev. A* **105**, 032415 (2022).
- [52] Hua Wei, ZhiJiao Deng, XiaoLong Zhang, and Mang Feng. “Transfer and teleportation of quantum states encoded in decoherence-free subspace”. *Phys. Rev. A* **76**, 054304 (2007).
- [53] Alejandro Fonseca. “High-dimensional quantum teleportation under noisy environments”. *Phys. Rev. A* **100**, 062311 (2019).
- [54] Xiao Xiao Hu, Fei Hao Zhang, Yan Song Li, and Gui Lu Long. “Optimizing quantum gates within decoherence-free subspaces”. *Phys. Rev. A* **104**, 062612 (2021).
- [55] D. Bacon, J. Kempe, D. A. Lidar, and K. B. Whaley. “Universal fault-tolerant quantum computation on decoherence-free subspaces”. *Phys. Rev. Lett.* **85**, 1758–1761 (2000).
- [56] Qiong Chen and Mang Feng. “Quantum-information processing in decoherence-free subspace with low-q cavities”. *Phys. Rev. A* **82**, 052329 (2010).
- [57] J. S. Pedernales, F. Cosco, and M. B. Plenio. “Decoherence-free rotational degrees of freedom for quantum applications”. *Phys. Rev. Lett.* **125**, 090501 (2020).
- [58] Arne Hamann, Pavel Sekatski, and Wolfgang Dür. “Approximate decoherence free subspaces for distributed sensing”. *Quantum Sci. Technol.* **7**, 025003 (2022).
- [59] Xin Wen Wang, Deng Yu Zhang, Shi Qing Tang, Li Jun Xie, Zhi Yong Wang, and Le Man Kuang. “Photonic two-qubit parity gate with tiny cross-kerr nonlinearity”. *Phys. Rev. A* **85**, 052326 (2012).
- [60] Io Chun Hoi, Anton F. Kockum, Tauno Palomaki, Thomas M. Stace, Bixuan Fan, Lars Tornberg, Sankar R. Sathyamoorthy, Göran Johansson, Per Delsing, and C. M. Wilson. “Giant cross-kerr effect for propagating

- microwaves induced by an artificial atom”. *Phys. Rev. Lett.* **111**, 053601 (2013).
- [61] Pieter Kok, W. J. Munro, Kae Nemoto, T. C. Ralph, Jonathan P. Dowling, and G. J. Milburn. “Linear optical quantum computing with photonic qubits”. *Rev. Mod. Phys.* **79**, 135–174 (2007).
- [62] Michael Siomau, Ali A. Kamli, Sergey A. Moiseev, and Barry C. Sanders. “Entanglement creation with negative index metamaterials”. *Phys. Rev. A* **85**, 050303 (2012).
- [63] Hanhee Paik, D. I. Schuster, Lev S. Bishop, G. Kirchmair, G. Catelani, A. P. Sears, B. R. Johnson, M. J. Reagor, L. Frunzio, L. I. Glazman, S. M. Girvin, M. H. Devoret, and R. J. Schoelkopf. “Observation of high coherence in josephson junction qubits measured in a three-dimensional circuit qed architecture”. *Phys. Rev. Lett.* **107**, 240501 (2011).
- [64] Gerhard Kirchmair, Brian Vlastakis, Zaki Leghtas, Simon E. Nigg, Hanhee Paik, Eran Ginossar, Mazyar Mirrahimi, Luigi Frunzio, S. M. Girvin, and R. J. Schoelkopf. “Observation of quantum state collapse and revival due to the single-photon kerr effect”. *Nature* **495**, 205–209 (2013).
- [65] M. D. Lukin and A. Imamoglu. “Nonlinear optics and quantum entanglement of ultra-slow single photons”. *Phys. Rev. Lett.* **84**, 1419–1422 (2000).
- [66] M. Bajcsy, A. S. Zibrov, and M. D. Lukin. “Stationary pulses of light in an atomic medium”. *Nature* **426**, 638–641 (2003).
- [67] Zeng Bin Wang, Karl Peter Marzlin, and Barry C. Sanders. “Large cross-phase modulation between slow copropagating weak pulses in ^{87}Rb ”. *Phys. Rev. Lett.* **97**, 063901 (2006).
- [68] Yi Hsin Chen, Meng Jung Lee, Weilun Hung, Ying Cheng Chen, Yong Fan Chen, and Ite A. Yu. “Demonstration of the interaction between two stopped light pulses”. *Phys. Rev. Lett.* **108**, 173603 (2012).
- [69] Hyunseok Jeong. “Quantum computation using weak nonlinearities: Robustness against decoherence”. *Phys. Rev. A* **73**, 052320 (2006).
- [70] Amir Feizpour, Xingxing Xing, and Aephraim M. Steinberg. “Amplifying single-photon nonlinearity using weak measurements”. *Phys. Rev. Lett.* **107**, 133603 (2011).
- [71] Seckin Sefi, Vishal Vaibhav, and Peter van Loock. “Measurement induced optical kerr interaction”. *Phys. Rev. A* **88**, 012303 (2013).
- [72] Monika Bartkowiak, Lian Ao Wu, and Adam Miranowicz. “Quantum circuits for amplification of kerr nonlinearity via quadrature squeezing”. *J. Phys. B: At. Mol. Opt. Phys.* **47**, 145501 (2014).
- [73] Holger F Hofmann, Kunihiro Kojima, Shigeki Takeuchi, and Keiji Sasaki. “Optimized phase switching using a single-atom nonlinearity”. *J. Opt. B: Quantum Semi-class. Opt.* **5**, 218 (2003).
- [74] Christoffer Wittmann, Ulrik L. Andersen, Masahiro Takeoka, Denis Sych, and Gerd Leuchs. “Discrimination of binary coherent states using a homodyne detector and a photon number resolving detector”. *Phys. Rev. A* **81**, 062338 (2010).
- [75] Li Dong, Jun Xi Wang, Qing Yang Li, Hong Zhi Shen, Hai Kuan Dong, Xiao Ming Xiu, Ya Jun Gao, and Choo Hiap Oh. “Nearly deterministic preparation of the perfect w state with weak cross-kerr nonlinearities”. *Phys. Rev. A* **93**, 012308 (2016).
- [76] Michael A. Nielsen and Isaac L. Chuang. “Quantum computation and quantum information”. Cambridge University Press. (2010).